Plasma Phys. Control. Fusion **40** (1998) 2081–2095. Printed in the UK PII: S0741-3335(98)94734-0

Trials of RF plasma production using different antenna geometries with magnetic field

Shunjiro Shinohara† and Tsutomu Soejima

Interdisciplinary Graduate School of Engineering Sciences, Kyushu University, Kasuga, Fukuoka 816-8580, Japan

Received 1 June 1998, in final form 18 September 1998

Abstract. Plasma production studies excited by the radio frequency (RF) wave were carried out using various antenna configurations. Six types of side antennae, located outside the large cylindrical chamber, and two types of internal loop antennae were tested. The ion saturation current I_{is} of a probe and the plasma emission were measured as a function of the filling pressure, the RF power and the magnetic field. With the increase in the power and the magnetic field, I_{is} increased in most cases, while some of the antennae showed the maximum I_{is} values under low magnetic field. Among the side antennae, a spiral antenna produced the highest value of I_{is} in a wide operational window. For the case of the internal loop antennae, the electric field parallel to the magnetic field did not show a significant contribution to plasma production. These results suggest the importance of the loop-like RF-induced electric field. When an external magnetic field was applied, the uniformity of the plasma produced by the internal loop antennae in both the radial and axial directions was improved.

1. Introduction

High-density plasmas generated at low filling pressure are urgently required for material processing applications and toroidal confinement devices. In order to fulfil the requirements of applications such as dry etching, inductively coupled plasma (ICP)/transformer coupled plasma (TCP) sources [1] and a helicon wave plasma [2–9] have been actively developed using radio frequency (RF) power sources. In ICP sources, a planar spiral coil [10, 11] has been used due to its relatively simple geometry, and the addition of an external magnetic field has led to better plasma performance [12–15]. As for the nuclear fusion field, in stellarators, plasma production studies have been performed in the ion cyclotron range of frequencies (ICRF) using slot and three half-turn antennae located outside the chamber [16–18]. More recently, ICRF plasma production for the purpose of wall conditioning, preionization and plasma sustainment has been performed in stellarators and tokamaks using the conventional loop antennae located inside the chamber [19–23]. The RF range has some advantages compared to other regimes, such as the microwave frequency range, due to the possible use of the continuous frequency with cheaper sources and the easier operation, and in some cases, a lower sensitivity of plasma production efficiency to the magnetic field.

In most previous applications, plasma sources which used RF antennae were of two types. In the first type, an antenna is located at the end of a cylindrical chamber, and power is coupled through a dielectric window. In the second type, an antenna is wound around the

† E-mail address: sinohara@aees.kyushu-u.ac.jp

0741-3335/98/122081+15$19.50

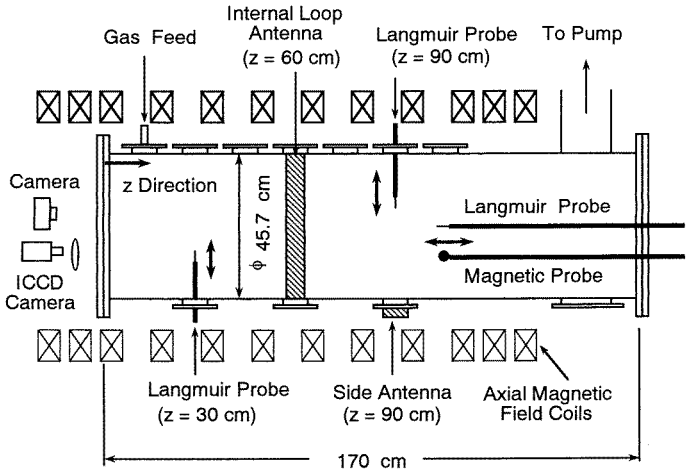

Figure 1. Schematic view of the experimental device.

outside of a non-metal cylindrical tube, with a diameter that is typically less than 10 cm. There are few results for discharges generated by antennae outside the side windows of the chamber. In some cases, internal antennae have been used, but the near fields such as the capacitive field must be minimized [24] in order not to have parasitic effects on the plasma performance.

However, there have been few trials of changing the antenna configurations within a limited set of conditions constrained by the device geometry, considering an external magnetic field, which affects excited wave field phenomena, plasma production and loss rates. Therefore, finding some innovative RF plasma production method utilizing the limited size of the window, positioned either at the side or the end, can be considered to be very important. This simple and easy plasma production method also gives the possibility of trimming the plasma profile, especially in the outer plasma region, which is related to crucial parameters such as plasma uniformity. Understanding the role of the axial and azimuthal electric fields as well as the external magnetic field for the case of an internal antenna can also be considered to be important for the optimum design of plasma reactors.

Here in this paper, we focus on experimental studies of RF plasma production using various types of antennae, which are located either outside of the chamber (at the side) or internally. Section 2 contains a brief description of an experimental set-up. In section 3, experimental results are presented, mainly of ion saturation currents, measured using a probe, for each antenna type. External parameters, such as the RF power, the filling pressure and the magnetic field, were varied, and the role of the electric field components was considered. Measurements of the excited fields and the plasma light are also described. Finally, a discussion and conclusions are presented in sections 4 and 5, respectively.

2. Experimental set-up

The linear device used in our experiments is shown in figure 1. The large cylindrical chamber had a diameter of 45.7 cm. A static axial magnetic field B of up to 1000 G was applied, and the RF frequency and incident power P_{in} (power reflection ratio $<20\%$) were 7 MHz and $\leqslant$1500 W, respectively. The RF pulse width was 2 ms with a duty of <0.07.

The side and internal loop antennae were positioned at $z = 90$ and 60 cm, respectively, where z was taken from the inner left surface of the vacuum chamber along the centre axis. The plasma was operated in argon gas, with a pressure P_0 in the range 0.8–16 mTorr, and plasma parameters were measured by movable Langmuir probes inserted into the plasma radially and axially. The excited wave fields were measured by a movable magnetic probe, and a balanced mixer for the interferometric wave measurement and a boxcar integrator were also used. The plasma light was monitored by an ICCD camera (a CCD camera with an image intensifier) and by a conventional camera.

Figure 2 shows the antenna structure of the side antennae, which were put on the outer surface of the quartz window, which was 28.6 cm high, 12.8 cm wide and 1 cm thick. The height and width of the flange hole were 25 cm and 9.2 cm, respectively. The distance between the antenna and the inner surface of the main chamber was 3.7 cm. For checking the role of the electric field components, six types of antennae made of copper with 0.03 cm thickness were used. The E_z crank and E_z ladder antennae, shown in figures 2(a) and 2(b), induce mainly the z component of the electric field in cylindrical geometry. The E_θ crank, E_θ ladder and E_θ rectangular antennae, shown in figures 2(c)–(e), induce mainly the azimuthal θ component of the electric field. The spiral antenna, shown in figure 2(f), which has a mixture of z and θ components, generates the radial component of the oscillating magnetic field. Note that the E_z crank (E_θ crank) antenna also has a non-negligible component of the E_θ (E_z) induced field.

Figure 3 shows two types of loop antennae (made of copper of 0.03 cm thickness) which were placed inside the vacuum chamber. The rectangular loop is a conventional E_θ induction antenna and the E_z crank loop, which has 32 parallel (to the axis) elements, can induce the E_θ field component as well as the E_z one. These two antennae were covered by flexible Teflon plate of 0.038 cm thickness, in order to reduce electrostatic coupling.

3. Experimental results

3.1. Side antennae

The Langmuir probe used to measure plasma parameters was located at the same axial position of the antenna ($z = 90$ cm) at a radial distance of 3.7 cm from the antenna. The electron temperature T_e, which was in the range of 3–4 eV, did not change appreciably regardless of the antenna shape and the magnetic field for $P_{in} = 1000$ W and $P_0 = 16$ mTorr.

Figures 4 and 5 show the ion saturation current I_{is} as a function of P_{in} and the axial magnetic field B, respectively, changing P_0 for the E_z crank antenna case. In this case, $I_{is} = 1000$ corresponds to the electron density $n_e = 4 \times 10^{10}$ cm^{-3} if we take $T_e = 3$ eV. With an increase in P_{in} and/or B, I_{is} increased, and $n_e = 5.8 \times 10^{10}$ cm^{-3} (under the assumption of $T_e = 3$ eV) was obtained for the plasma conditions of $P_{in} = 1500$ W, $B = 1000$ G and $P_0 = 16$ mTorr. The plasma could not be generated in low-B and low-P_0 conditions, and I_{is} decreased for values of B above a critical field B when P_0 was low, even though a plasma was produced. The e-folding length along the radial direction was <10 cm, and this length became shorter gradually as B increased. This is mainly a result of the reduction of radial diffusion.

For the cases of the E_z ladder and E_θ crank antennae, the dependences of I_{is} on P_{in}, B and P_0 was similar to those of the E_z crank antenna case. However, for the case of the E_z ladder antenna, the absolute value of I_{is} was smaller by about a factor of two. This may be partly due to the fact that, for the E_z ladder antenna case, the RF antenna current flowed mainly near the central elements and the top and bottom ones had small antenna currents

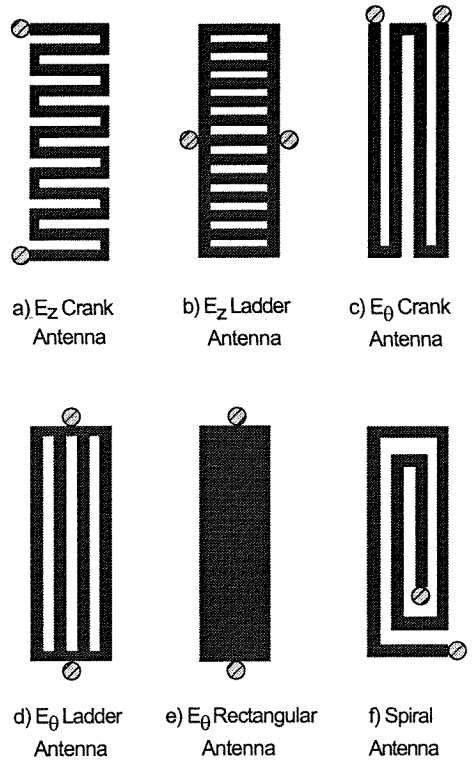

Figure 2. The various types of side antennae which were used: (a) E_z crank, (b) E_z ladder, (c) E_θ crank, (d) E_θ ladder, (e) E_θ rectangular and (f) spiral shapes. The RF feeding points are indicated as closed circles.

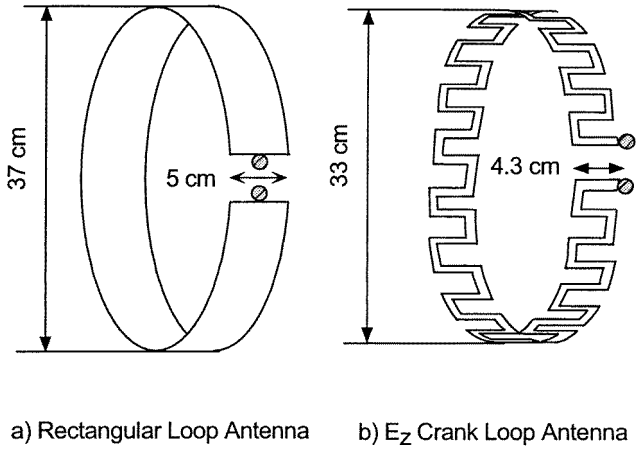

Figure 3. The two types of internal loop antennae which were used: (a) rectangular and (b) E_z crank loops. The RF feeding points are indicated as closed circles.

(see RF feeding points in figure 2(b)). This means that this antenna has a smaller effective antenna area than those of the other two. Here, for convenience, we define the above three types of the antennae as group A.

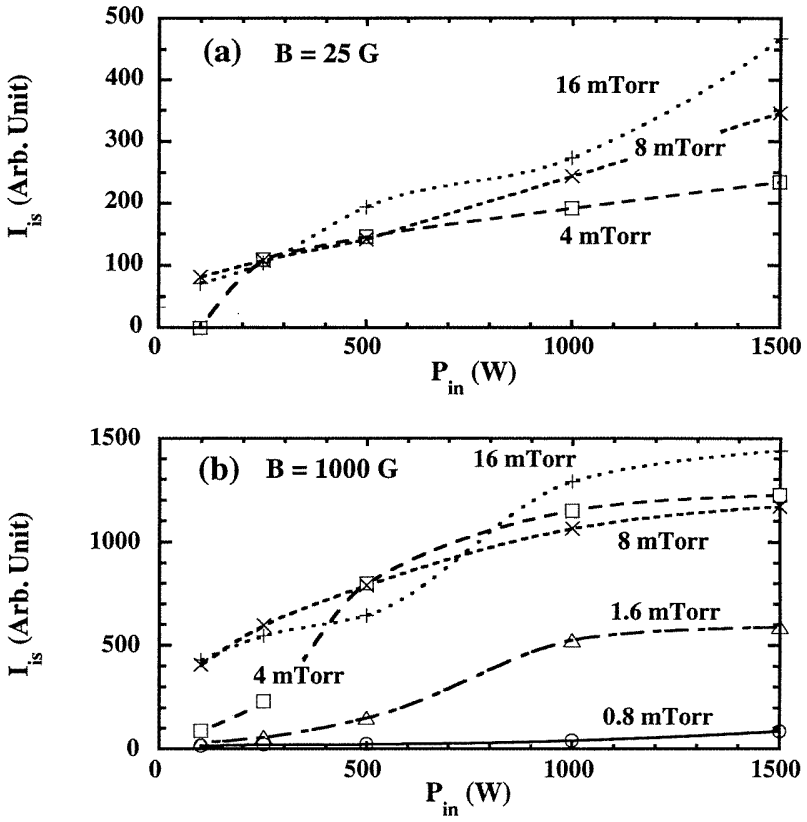

Figure 4. Ion saturation current I_{is} as a function of the RF input power P_{in}, for different filling pressures P_0 for discharges excited by the E_z crank antenna with an applied magnetic field of (a) $B = 25$ G and (b) $B = 1000$ G.

In contrast, for the cases of the E_θ ladder, E_θ rectangular and spiral antennae (they are categorized as group B), the dependences of I_{is} on B and P_{in} were different from the group A antennae except for in low-P_{in} and high-B conditions. Figures 6 and 7 show I_{is} as a function of P_{in} and B, respectively, changing P_0 for the E_θ ladder antenna case. When $B = 25$ G, $P_{in} > 500$ W and P_0 was greater than a few mTorr, I_{is} became high and increased with increasing P_{in} and P_0 noticeably, and the highest value of n_e obtained was 2.8×10^{11} cm^{-3} (if we take $T_e = 3$ eV). The rectangular and spiral antennae showed similar results as the E_θ ladder antenna in that I_{is} was higher in plasmas with low B. This feature can be seen clearly for the case of high P_{in} (see, e.g., figure 7(b)). The spiral antenna exhibited the best performance for plasma generation among the group B antennae, as shown by the results in figures 8 and 9; the plasma production window in P_{in}, B and P_0 space was wide, and n_e was as high as 4.4×10^{11} cm^{-3} (if we take $T_e = 3$ eV) for the plasma conditions of $P_{in} = 1500$ W, $B = 25$ G and $P_0 = 16$ mTorr. In the high-B-field region of more than a few hundreds of G, I_{is} in the group B antennae was the nearly the same as the E_z crank antenna case, while in the low-field region I_{is} was higher. Note that under the condition that $B = 0$ G, no successful plasma initiation was found for all cases of the side antennae (groups A and B).

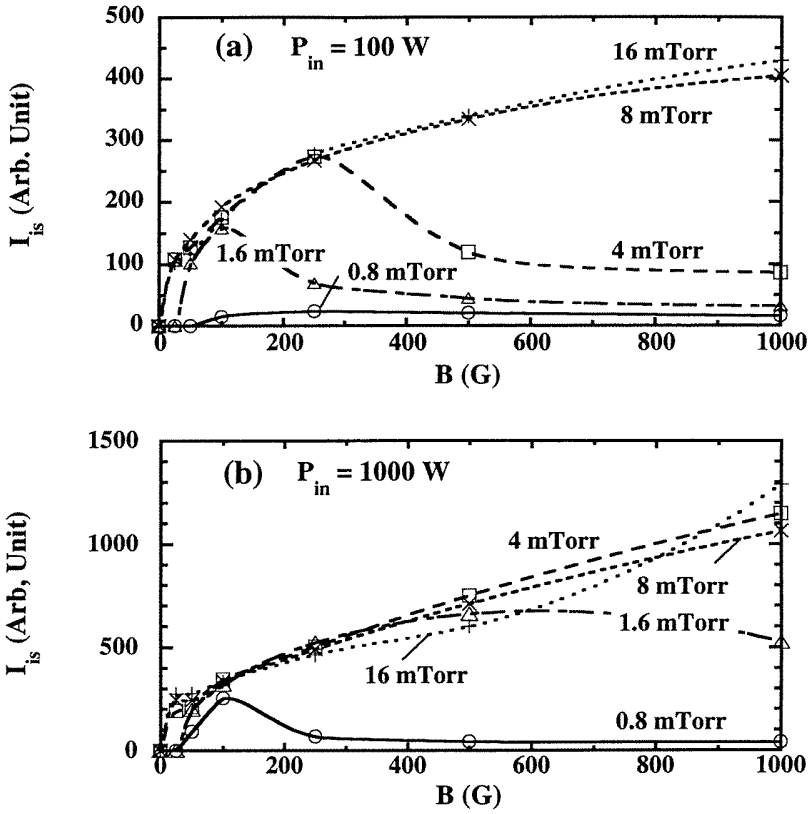

Figure 5. Ion saturation current I_{is} as a function of the magnetic field B, for different filling pressures P_0 for discharges excited by the E_z crank antenna with input power of (a) $P_{in} = 100$ W and (b) $P_{in} = 1000$ W.

The power coupling efficiency η can be defined as $R_p/(R_p+R_c)$, where R_c and R_p denote the vacuum and plasma loading resistances, respectively. In this expression, the antenna loading ($= P_{in}$ divided by the square of the effective RF antenna current) is expressed as $R_p + R_c(R_c)$ in the presence (absence) of the plasma. The values of η were $\sim$0.72 for the spiral antenna (this value decreased slightly with increasing B), $\sim$0.6 for the E_z crank antenna, $\sim$0.55 for the E_θ crank and rectangular antennae, and $\sim$0.5 for the E_z ladder and E_θ ladder antennae for the plasma conditions of $P_{in} = 1000$ W, $B = 25$ G and $P_0 = 16$ mTorr. These results show the slight differences of η between various antennae compared with the I_{is} value. The plasma light measurements by the ICCD camera showed the consistent result that higher plasma intensity with a wider emitting region was obtained for discharges in which a higher value of I_{is} was obtained. Due to the incomplete shielding at the RF feeder position, the plasma light intensity was also higher near this position (high RF voltage side).

3.2. Internal loop antennae

The ion saturation current I_{is} was measured in the centre of the vacuum chamber (radial position $r = 0$ cm) at the same axial position as the loop antennae ($z = 60$ cm). Figure 10

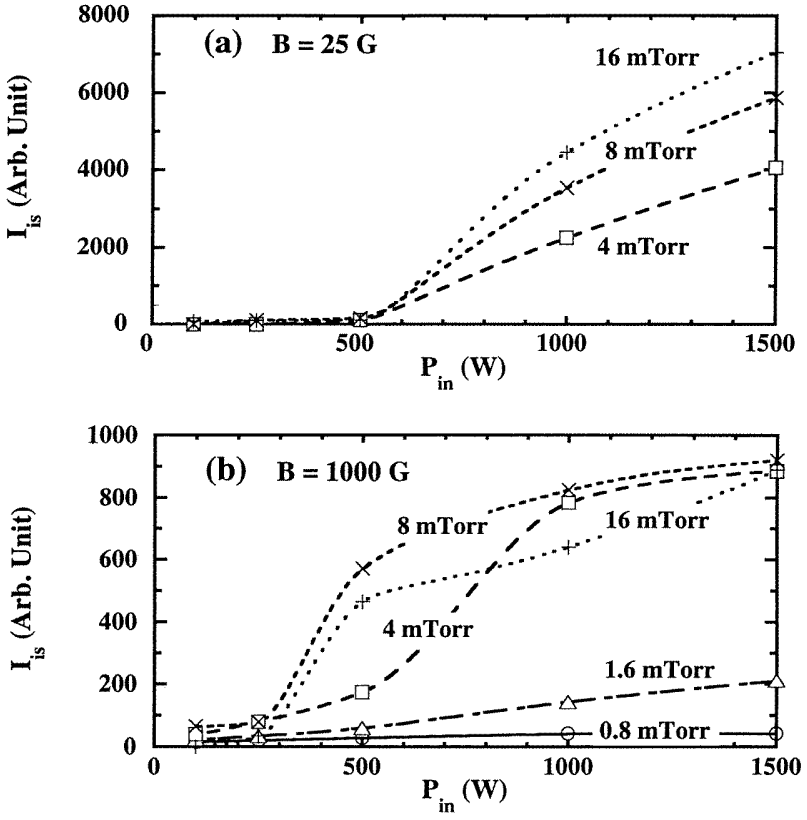

Figure 6. Ion saturation current I_{is} as a function of the RF input power P_{in}, for different filling pressures P_0 for discharges excited by the E_θ ladder antenna with an applied magnetic field of (a) $B = 25$ G and (b) $B = 1000$ G.

shows the relationship between I_{is} and B, measured for different values of P_0 using the E_z crank loop antenna. In this figure, $I_{is} = 1000$ again corresponds to $n_e = 4 \times 10^{10}$ cm^{-3} if we take $T_e = 3$ eV. For the case of $B = 0$ G at the lower pressures of $P_0 = 0.8$ and 1.6 mTorr, the plasma was not initiated. However, in the higher pressure regimes of $P_0 = 8$ and 16 mTorr, I_{is} was higher without the magnetic field than with the field. This tendency can be clearly seen for the higher RF power case (see figure 10(b)). With the increase in P_{in}, I_{is} increased almost linearly from $P_{in} = 100$ to 1000 W, and I_{is} was relatively higher for the higher pressure case. The dependences of I_{is} on P_{in}, B and P_0 including absolute values of I_{is} (and also the radial and the axial distributions of I_{is} described after) were nearly the same for both the rectangular loop and the E_z crank loop antennae.

The radial distribution of I_{is} was measured at $z = 30$ cm, which was 30 cm from the antennae in the axial direction. Figure 11 shows one example obtained with the E_z crank loop antenna for different magnetic field values. Without the magnetic field, I_{is} was higher but had a round shape profile. On the other hand, when the magnetic field was applied, I_{is} became uniform with lower values; the effective diameter D_{eff}, defined as the region where I_{is} is uniform within $\pm 7\%$, was $\sim$30 cm for $B = 100$ G. Above $B = 100$ G the central value of I_{is} was unchanged, while near the edge region it increased with the increase in B. The higher values of I_{is} which can be seen at the negative radial position

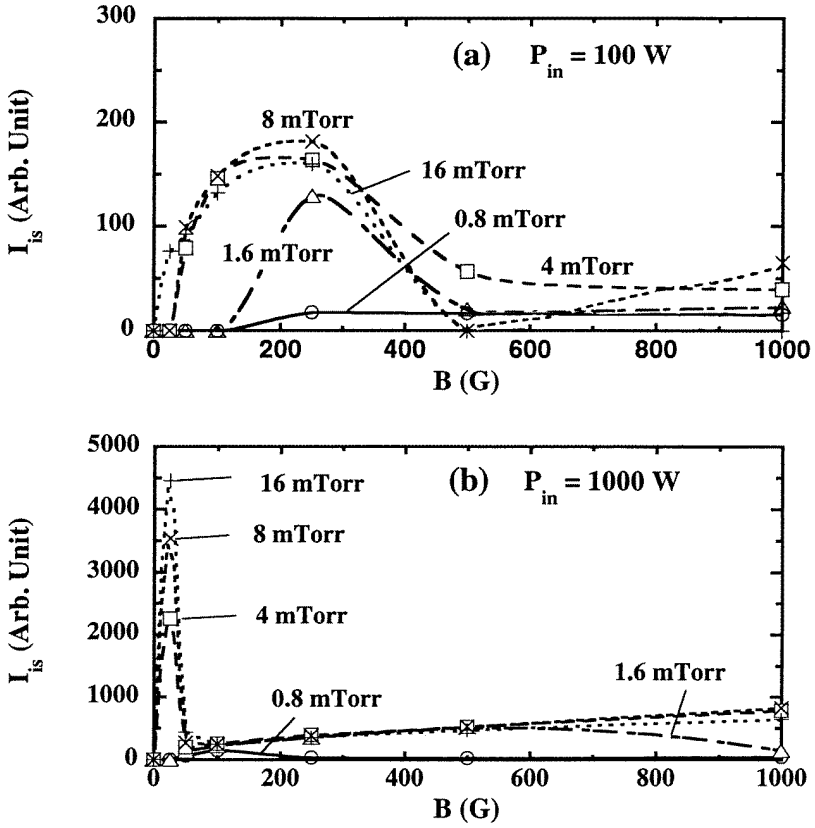

Figure 7. Ion saturation current I_{is} as a function of the magnetic field B, for different filling pressures P_0 for discharges excited by the E_θ ladder antenna with input power of (a) $P_{in} = 100$ W and (b) $P_{in} = 1000$ W.

reflected the insufficient shielding at the feeder position (high RF voltage side). The plasma light intensity was also higher at this position, and a similar feature was observed with the side antennae. This intensity distribution obtained by the camera was broad for discharges without an applied magnetic field, and with an increase in B, the region of high plasma light intensity became localized at the antenna position, which is consistent with the Langmuir probe results.

The reason for the change of the radial profile of I_{is} due to the addition of an external magnetic field, as seen in figure 11, can be considered to be that the plasma produced near the antenna region was also confined in this region by the presence of the magnetic field, due to low radial diffusivity. For the case of discharges without a magnetic field, the plasma production region was larger, due to the higher diffusivity. Previously published results obtained with a four-turn spiral antenna [13] located on the outer left-hand side of the chamber (the end section) indicated that the central value of I_{is} was larger and a more peaked radial profile was obtained with $B = 36$ G compared with the values obtained for a discharge without a magnetic field. The difference between those results and the present results is due to the different radial characteristics of the antenna; the spiral antenna used in the previous research was wound with four turns within a diameter of $\sim$18 cm, and so

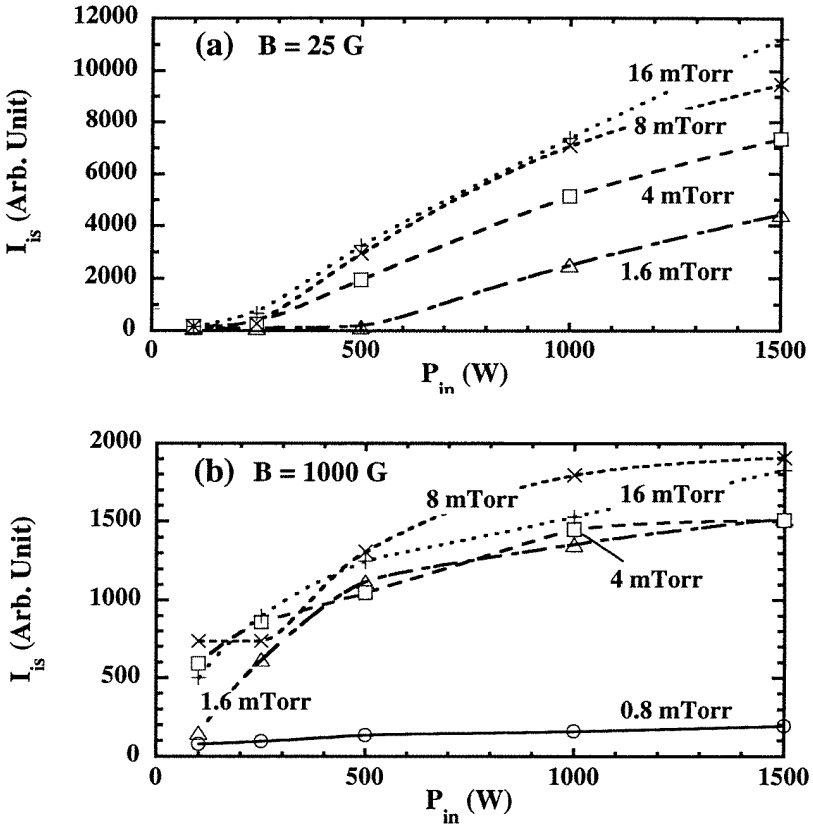

Figure 8. Ion saturation current I_{is} as a function of the RF input power P_{in}, for different filling pressures P_0 for discharges excited by the spiral antenna with an applied magnetic field of (a) $B = 25$ G and (b) $B = 1000$ G.

the plasma production region was near the centre of the vacuum chamber. In the present case, the E_z crank loop antenna (one turn) has a diameter of 33 cm (see figure 3), and so the plasma is produced in the outer region of the chamber.

Figure 12 shows the axial distribution of I_{is} at $r = 0$ cm, for discharges produced with the rectangular loop antenna. For the case of the lower pressure of $P_0 = 1.6$ mTorr, I_{is} decreased with increasing B ($B \geqslant 250$ G), and no plasma production was found without the applied magnetic field. For the higher pressure case of $P_0 = 8$ mTorr, I_{is} was not changed appreciably regardless of the magnetic field strength ($B \geqslant 100$ G), while the more peaked profile and higher values of I_{is} were obtained with $B = 0$ G, which has the same tendency as the radial distribution of I_{is} (see figure 11).

In order to check the wave propagation along the axial direction, measurements of the excited magnetic field were made. The excited field (B_r component in the intermediate radius of the chamber) was fairly constant in an extended region, up to $\sim$20 cm along the axial direction, and then decayed with an e-folding length of $<$5 cm. There was a tendency for the extended region and the decay length to become longer as B was increased. For our experimental conditions, the most likely candidate for the propagating wave is the whistler wave (see also the discussion in section 4), also known as the helicon wave, but

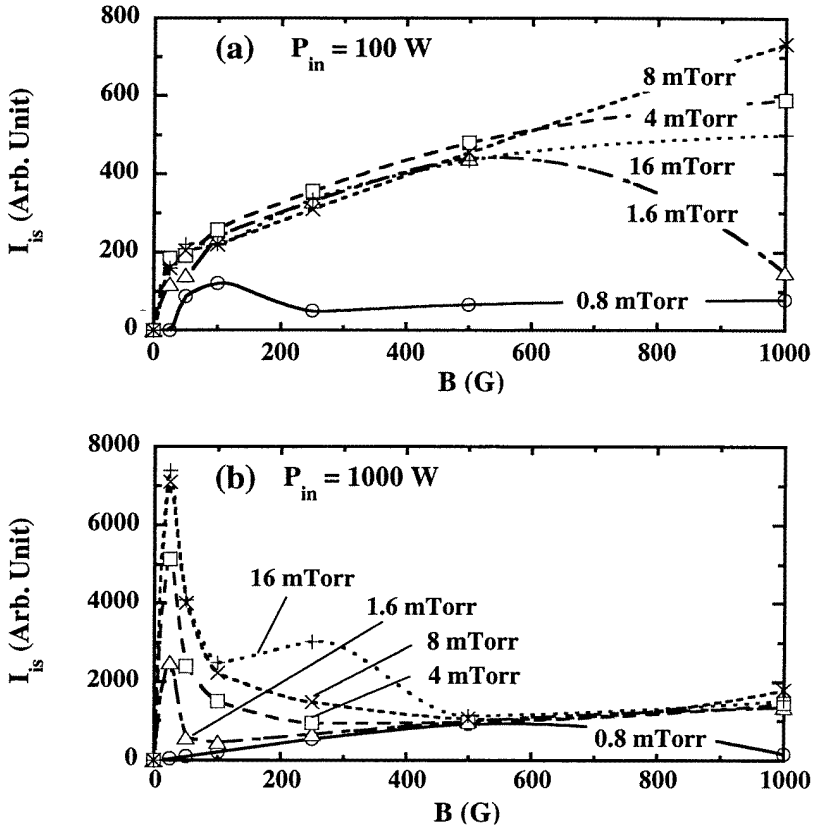

Figure 9. Ion saturation current I_{is} as a function of the magnetic field B, for different filling pressures P_0 for discharges excited by the spiral antenna with input power of (a) $P_{in} = 100$ W and (b) $P_{in} = 1000$ W.

the estimated wavelength of this wave when n_e is of the order of $\times 10^{10}$ cm^{-3} is more than several metres, which is larger than the device size in the axial direction. In fact, additional wave measurements, made at different phases of the excited wave, indicated that a standing wave was found regardless of the magnetic field strength. Recent experiments [6, 8, 25] in which waves of different azimuthal mode numbers $m = 1, 0, -1$ were excited in a small diameter plasma showed that a standing wave existed near the antenna, while a propagating helicon wave was found outside it. A distance of roughly more than a quarter wavelength was necessary for the wave to propagate [25]. Therefore, it is difficult to measure the wave propagation in the present experiment even if the whistler wave was excited.

4. Discussion

First, we will consider the penetration of the electric field into the plasma. For the case of $n_e = 4 \times 10^{10}$ cm^{-3}, which corresponds to $I_{is} = 1000$ (with the assumption of $T_e = 3$ eV), the classical skin depth c/ω_{pe} for the light and ordinary (O) waves is $\sim$2.7 cm, where c and ω_{pe} are the velocity of light and the electron plasma angular frequency, respectively. When P_0 is less than 16 mTorr with $T_e = 3$ eV, electron–neutral collisions (the collision frequency

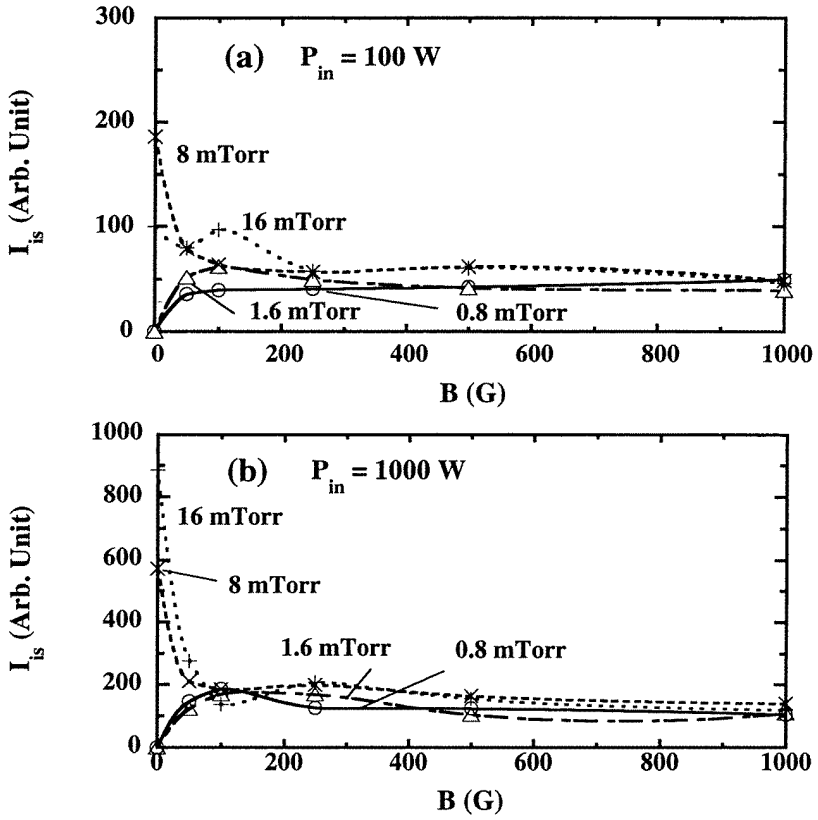

Figure 10. Ion saturation current I_{is} as a function of the magnetic field B, for different filling pressures P_0 for discharges excited by the E_z crank loop antenna with input power of (a) $P_{in} = 100$ W and (b) $P_{in} = 1000$ W.

is denoted as ν) are dominant compared with Coulomb collisions between electrons and ions. The value of ν/ω is less than 1 (ω is the excited angular RF frequency), which leads to the correction factor f_c of the skin depth from the c/ω_{pe} term being less than 1.2 [26]. The electron thermal effect [27], the so-called anomalous skin effect, can be neglected for high P_0 conditions.

Among the various waves [28] with the parallel (right-hand (R) and left-hand (L) circularly polarized waves) and perpendicular (ordinary and extraordinary (X) waves) directions of the wavevector with respect to the magnetic field, light and O waves are evanescent with the above-mentioned skin depth, and the R wave (whistler wave) is the propagating wave for our experimental conditions. The L and X waves are evanescent in a low magnetic field, but the L wave can propagate into a low-density plasma if the magnetic field increases (e.g., for conditions such as $n_e < 2.4 \times 10^8$ cm^{-3} for $B = 1000$ G). The lower hybrid frequency is close to the excited RF frequency when $B \sim 680$ G, and above this magnitude field strength the window of the propagating X wave appears at high plasma density (e.g., for conditions such as $n_e > 8.3 \times 10^{10}$ cm^{-3} for $B = 1000$ G). The maximum value of f_c is more than several times when B is stronger than several hundreds of G with relatively high n_e in our experiments [26]. According to [29], the parallel and perpendicular

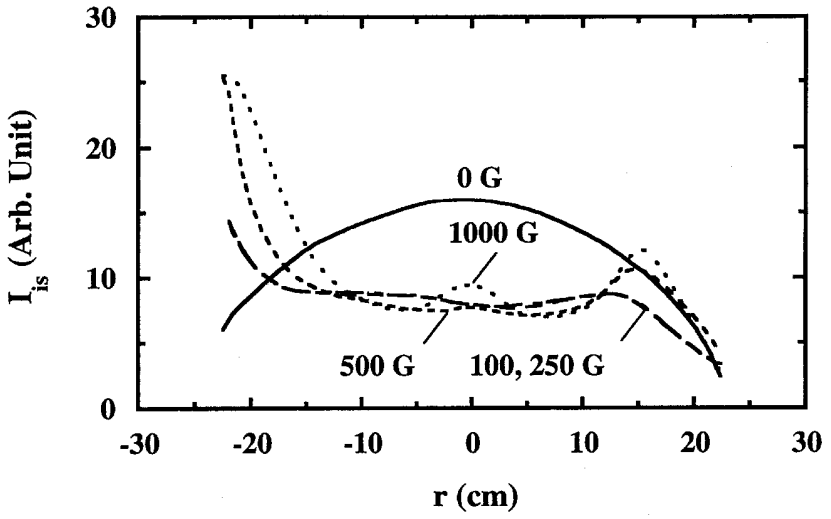

Figure 11. Radial distribution of I_{is} at $z = 30$ cm, for different applied magnetic fields for discharges excited by the E_z crank loop antenna with input power $P_{in} = 250$ W and filling pressure $P_0 = 8$ mTorr.

skin depths are inferred from the conductivity along and across the magnetic field with some assumptions; they concluded that the perpendicular skin depth is larger than the parallel one by roughly ω_{ce}/ω. This factor becomes large ($\sim$400) in our experiments with $B = 1000$ G, and it leads to a perpendicular skin depth which is larger than our chamber diameter by up to one order of magnitude. This is unlikely to occur and we had no indication of plasma production across the radius in the inner vacuum chamber.

As for the plasma production mechanism, collisional damping is considered to be dominant compared with other dampings, such as the lower hybrid resonance and the electron Landau damping. We did not have a clear indication of any correlation of I_{is} with B near the lower hybrid frequency and there might be a small window to have the matching condition of the phase velocity and the electron thermal velocity for the Landau damping. For the low-P_0 case, collisionless damping [27] may also contribute to the plasma production. From the above discussions of the skin depth and plasma production, we may conclude as follows: the plasma was mainly produced near the side antenna by an evanescent wave with f_c ranging from unity to several and by a whistler wave due to mainly collisional damping, and the plasma density increased with the magnetic field due to the smaller diffusivity across the radius.

The reason why the plasma density was higher in the group B, especially for discharges with low magnetic field, is unclear. The decrease in I_{is} above a certain value of B was somewhat similar for the case excited by a four-turn spiral antenna [15], in which the plasma could not be initiated above $B = 150$–200 G and the amplitude of the excited helicon wave saturated at $B > \sim 100$ G. When we consider the antenna wavenumber spectrum, the E_z (E_θ) crank antenna has the first peak of $j_z(k_\theta)(j_\theta(k_z))$ at finite $k_\theta \sim 1.7$ cm^{-1} ($k_z \sim 1.6$ cm^{-1}) and zero at $k_\theta(k_z) = 0$ cm^{-1}. Here, we define $j(k)$ as the Fourier spectrum of the antenna current j (k and the suffix show the wavenumber and the component in cylindrical geometry, respectively). In contrast, the E_θ ladder and E_θ rectangular antennae have a maximum of $j_\theta(k_z)$ at $k_z = 0$ cm^{-1} and decrease with k_z. Although we did not observe the so-called density jump (i.e. a steep increase in density above a threshold P_{in}

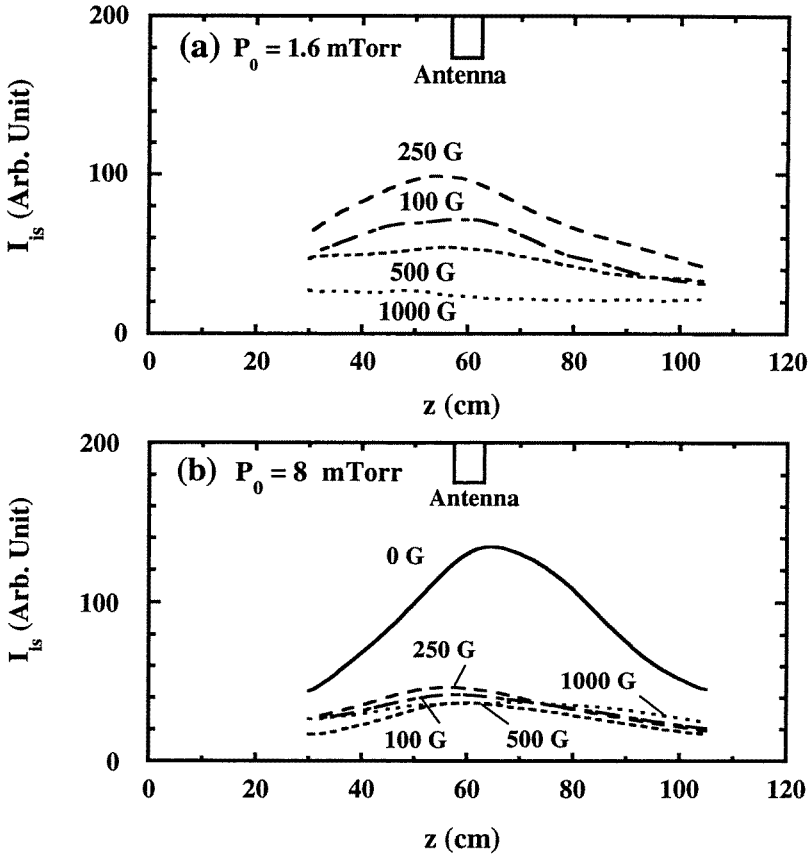

Figure 12. Axial distribution of I_{is} in the plasma centre of $r = 0$ cm, for different applied magnetic fields for discharges excited by the rectangular loop antenna with input power $P_{in} = 500$ W and a filling pressure of (a) $P_0 = 1.6$ mTorr and (b) $P_0 = 8$ mTorr.

value), the present results with the above features of the antennae spectra are similar with previous helicon wave results [25]. In that case, for the $m = 0$ mode excitation with a small loop antenna wound around the tube, which was 5 cm in diameter, the P_{in} and P_0 space for plasma initiation and for obtaining high-density plasma by the helicon wave was wider when the low-wavenumber (k_z) spectrum part became larger.

As for the cancellation of the excited electric field, it is smaller for the group B antennae than for the group A antennae (except for the E_z ladder antenna), since the distance between the neighbouring elements having opposite currents in group A was smaller than the typical skin depth, especially for the low-density case. This effect may play an important role for plasma production. Needless to say, the finite size of the side port may also affect the excited RF electric field because of the tight location of the antennae in the port section. Note that the spiral antenna has a loop-like pattern of the electric field without the significant electric field cancellation and can induce the oscillating radial magnetic field.

Between the rectangular loop and the E_z crank loop antennae, as was presented, the parameter dependences and also the radial and axial distributions of I_{is} were similar to each other. This shows that the E_z component was not so important for plasma generation but the E_θ component, in other words the loop-like E_θ electric field pattern, played an important

role for the production, as was the case for the side antennae. However, there may be a cancelling effect of the E_z component between the neighbouring opposite current elements due to the relatively large skin depth mentioned above.

Note that, although an RF frequency of 7 MHz was used throughout our experiments, the obtained dependences of plasma parameters such as I_{is} on the external parameters may not change appreciably with RF frequency, as long as the antenna size is much smaller than the RF wavelength in free space and the wave resonance condition is not satisfied.

From the experimental results presented here, for designing a new antenna, regardless of the antenna position and its shape, it is very important to consider the loop-like RF electric field and/or the reduction of the cancellation effect of the electric field from the neighbouring RF current elements, which are also related to the wavenumber spectrum. Needless to say, the increase in the effective antenna area may improve the efficiency of the plasma production, and the effect of the feeder part of the antenna must be minimized. In addition, the skin depth of the individual components of the excited electric field in the plasma for the case of the evanescent wave, and the condition for the excitation of the propagating wave, must be taken into consideration.

5. Conclusions

Plasma production studies excited by the RF wave with frequency of 7 MHz were carried out, using six types of side antennae, located outside the large cylindrical chamber with a diameter of 45.7 cm, and two types of internal loop antennae. The discharge was operated in argon at pressures P_0 ranging from 0.8 to 16 mTorr. With increasing RF power ($P_{in} \leqslant 1500$ W) and magnetic field ($B \leqslant 1000$ G), I_{is} generally increased for the group A antennae (E_z crank, E_z ladder and E_θ crank antennae), while the group B antennae (E_θ ladder, E_θ rectangular and spiral antennae) and also the rectangular loop and E_z crank loop internal antennae showed maximum I_{is} values for low values of the magnetic field ($B < 100$ G typically).

The spiral antenna demonstrated the highest I_{is} value over a wide operational window (P_{in}, P_0 and B) for the plasma production among the side antennae; the maximum n_e was as high as 4.4×10^{11} cm^{-3} if we take $T_e = 3$ eV. In addition, the E_z electric field component for the internal loop antenna case did not show a significant contribution to plasma production. These results suggest the importance of the loop-like RF-induced electric field and/or the reduction of the cancelling effect between the neighbouring RF current elements. When a magnetic field was applied to discharges excited by the internal loop antennae, the uniformity of the plasma distribution along the radial and axial directions was improved; the effective diameter D_{eff} (I_{is} was within $\pm7\%$) was up to $\sim$30 cm.

Acknowledgments

We would like to thank Professor Y Kawai for his continuous encouragement and Dr M D Bowden for checking the English.

References

[1] Hopwood J 1992 *Plasma Sources Sci. Technol.* **1** 109
[2] Boswell R W 1984 *Plasma Phys. Control. Fusion* **26** 1147
[3] Chen F F 1991 *Plasma Phys. Control. Fusion* **33** 339
[4] Shoji T, Sakawa Y, Nakazawa S, Kadota K and Sato T 1993 *Plasma Sources Sci. Technol.* **2** 5

[5] Yasaka Y and Hara Y 1994 *Japan. J. Appl. Phys.* **33** 5950
[6] Shinohara S, Miyauchi Y and Kawai Y 1995 *Plasma Phys. Control. Fusion* **37** 1015
[7] Shinohara S and Kawai Y 1995 *Japan. J. Appl. Phys.* **34** L1571
[8] Shinohara S, Miyauchi Y and Kawai Y 1996 *Japan. J. Appl. Phys.* **35** L731
[9] Shinohara S 1997 *Japan. J. Appl. Phys.* **36** 4695 and references therein
[10] Hopwood J, Guarnieri C R, Whitehair S J and Cuomo J J 1993 *J. Vac. Sci. Technol.* A **11** 147
[11] O'Neil J A, Barnes M S and Keller J H 1993 *Appl. Phys. Lett.* **73** 1621
[12] Stevens J E, Sowa M J and Cecchi J L 1995 *J. Vac. Sci. Technol.* A **13** 2476
[13] Shinohara S, Takechi S and Kawai Y 1996 *Japan. J. Appl. Phys.* **35** 4503
[14] Takechi S, Shinohara S and Kawai Y 1997 *Japan. J. Appl. Phys.* **36** 4558
[15] Shinohara S, Takechi S, Kaneda N and Kawai Y 1997 *Plasma Phys. Control. Fusion* **39** 1479
[16] Shvets O M, Kalinichenko S S, Lysoivan A I, Nazarov N I, Slavnyi A S and Terasenko V F 1981 *Sov. J. Plasma Phys.* **7** 261
[17] Golovato S N *et al* 1988 *Phys. Fluids* **31** 3744
[18] Lysoivan A I *et al* 1995 *Fusion Eng. Design* **26** 185
[19] Koch R *et al* 1996 *Proc. 16th IAEA Conf. on Fusion Energy (Montreal, 1996)* vol 1, p 633
[20] de la Cal E and Gauthier E 1997 *Plasma Phys. Control. Fusion* **39** 1083
[21] Esser H G, Lyssoivan A, Freisinger M, Koch R, Van Oost G, Weschenfelder F and Winter J 1997 *J. Nucl. Mater.* **241–243** 861
[22] Hartmann D A, Cattanei G, Lyon J F, Plysnin V, the ICRF Group and the W7-AS Team 1997 *Proc. 24th Eur. Conf. on Control. Fusion and Plasma Phys. (Berchtesgaden, 1997)* vol 21A, part IV, p 1633
[23] Lyssoivan A I *et al* 1998 *Proc. 2nd Europhysics Topical Conf. on Radio Frequency Heating and Current Drive of Fusion Devices (Brussels, 1998)* vol 22A, p 85
[24] Sugai H, Nakamura K and Suzuki K 1994 *Japan. J. Appl. Phys.* **33** 2189
[25] Shinohara S, Kaneda N and Kawai Y 1998 *Thin Solid Films* **316** 139
[26] Shinohara S and Kawai Y 1996 *Japan. J. Appl. Phys.* **35** L725
[27] Turner M M 1993 *Phys. Rev. Lett.* **71** 1844
[28] Stix T H 1992 *Waves in Plasmas* (New York: American Institute of Physics)
[29] Degeling A, Mikhelson N, Boswell R and Sadeghi N 1998 *Phys. Plasmas* **3** 572